Surfaces and Interfaces 33 (2022) 102296

Contents lists available at ScienceDirect

Surfaces and Interfaces

journal homepage: www.sciencedirect.com/journal/surfaces-and-interfaces

Tunable anisotropic in-plane thermal transport of multilayer graphene induced by 2D empty space: Insights from interfaces

Xin Wu, Qiang Han *

Department of Engineering Mechanics, School of Civil Engineering and Transportation, South China University of Technology, Guangzhou, Guangdong Province 510640, People's Republic of China

ARTICLE INFO

Keywords:
Tunable anisotropy
Phonon thermal transport
2D empty space
Multilayer graphene
Molecular dynamics

ABSTRACT

The emergence of two-dimensional empty space (2D-ES) not only enriches the means of van der Waals integration, but also provides a new and reliable solution for structural design-driven performance modulation. Here, by applying the concept of 2D-ES-based periodic structure design to multilayer graphene, the large-range tunable in-plane anisotropic phonon thermal transport behavior was discovered by extensive molecular dynamics simulations. Through a series of in-depth frequency-dependent and in-and-out of plane decomposition phonon analysis, it is found that 2D-ES and its interfaces with different periodic properties exhibit exactly opposite effects on phonon thermal transport along two in-plane orientations, which is the fundamental reason for the existence of the above-mentioned anisotropic thermal transport and its modulation. These findings provide new insights into the realization of in-plane anisotropic thermal transport in quasi-2D materials, which may further inspire novel thermal management strategies.

1. Introduction

Since the beginning of the 21st century, the microelectronics industry, as a key area leading the third technological revolution, has strived to continue the myth of "Moore's Law", even if the pursuit of this goal has gradually become less obsessive in recent years [1]. As this industry continues to develop towards miniaturization and densification, two critical issues have become key to its further high-quality development: the selection of suitable low-dimensional nanomaterials, and the problem of thermal management which can be considered as the bottleneck for development. Firstly, from the material point of view, the low-dimensional nanomaterials represented by graphene, while playing their own excellent performance, together with the van der Waals (vdW) integration technology as a representative of the diversity of structural design means, has injected a strong vitality for the development of the field [2–6]. More importantly, while improving the performance of the device, densification also brings the fatal problem of overhigh local heat density, which is a critical ordeal for the lifetime and usage experience of the device. Taken together, it is significant and necessary to study the thermal transport properties of nanomaterials, and in fact, they have shown enough attraction in this regard.

Controlling the direction of heat flow in nanomaterials through their thermal transport anisotropy has been widely recognized as an effective way to achieve thermal management and design strategies. Anisotropic thermal transport means that for the same material, the heat flow exhibits different propagation velocities along its different orientations, which can often be achieved by structural design tools such as resonance effects, breaking symmetry, and so on [7–10]. Here, for ease of presentation, we define the two directions with anisotropic thermal conductivity as the fast axis and the slow axis, respectively, whose corresponding thermal conductivities are denoted as κ_f and κ_s, and thus the anisotropy ratio can be defined as $\gamma = \frac{\kappa_f}{\kappa_s}$. Recently, Kim et al. [9] achieved thermal conductivity anisotropy ratios up to 900 in multilayer MoS_2 by random interlayer rotation, and Chen et al. [11] found a large range of tunable thermal conductivity anisotropy ratios from about 4.0 to 12.0 in porous carbon foams. All of the above strongly anisotropic thermal conductivities depend to some extent on their own structural differences along the in-plane and out-of-plane directions, however, the anisotropy in the in-plane direction of two-dimensional (2D) materials and their derivatives is much less [12]. Black phosphorus, a typical 2D material with in-plane anisotropic thermal conductivity, but its γ can only reach about 3.3 [13], which is already high among 2D materials [14,15]. And in the transition metal dichalcogenides (TMDs) [16–20] and the transition metal carbides/nitrides (MXenes) [21], the in-plane γ is also usually only about 2.0.

Driven by vdW material integration technology, 2D empty space (2D-ES) in multilayer graphene, with a pair of edge dislocations in

* Corresponding author.
E-mail address: emqhan@scut.edu.cn (Q. Han).

https://doi.org/10.1016/j.surfin.2022.102296
Received 7 July 2022; Received in revised form 11 August 2022; Accepted 19 August 2022
Available online 24 August 2022

the angstrom scale cavities, has made achievements in several fields including molecular and ion transport in less than five years since it was proposed [22–24]. By applying periodic structural design concepts to the 2D-ES in multilayer graphene, a quasi-2D vdW structure with a grid layout can be formed, and such periodic structural design tools have also been proven to be effective elements for structural design-driven thermal transport performance modulation [25,26]. In addition, we have found in our previous work that the thermal conductivity across the 2D-ES exhibits the non-monotonicity and anomalous global maximum with the monotonic variation of the periodicity, which provides an opportunity and a basis for the present study on the anisotropy of the in-plane thermal conductivity [27].

In this work, we reported a large-range tunable anisotropy of the in-plane thermal conductivity in the multilayer graphene induced by periodic 2D-ES. Through extensive molecular dynamics (MD) simulations incorporating homogeneous non-equilibrium molecular dynamics (HNEMD) and non-equilibrium molecular dynamics (NEMD) and their respective spectral heat current (SHC) decomposition methods, it has been found that the nature of the periodic arrangement of 2D-ES and its interfaces is the key to tuning anisotropic thermal transport. Furthermore, taking advantage of the characteristics of different dominant frequency bands corresponding to the phonon crossing the 2D-ES in different relative directions during transport, as well as the advantages of quasi-2D structures in in-plane and out-of-plane decomposition analysis, a comprehensive and beneficial discussions have been made from property exploration to mechanism analysis.

2. Simulation and methodology

To some extent, the concept of two-dimensional empty space (2D-ES) was inspired by the process of preparing graphene by mechanical exfoliation. After exfoliating a single layer of graphene from a piece of graphite, attention is focused on the remaining part to obtain an angstrom-scale 2D-ES with a pair of edge dislocations. Thinking backwards about this process and using the smaller graphene strip as a spacer between two flat graphite (or graphene) layers, the result is precisely a multilayer graphene structure with the 2D-ES, which is the basic idea followed in the design and preparation of this class of 2D-ES structures. Fortunately, with the continuous development and maturity of vdW integration technology, such artificial vdW structures are no longer just at the level of our imagination. Further, this process can be simplified and understood as a stacking process of vdW components with different specifications according to certain rules, which also means that it will have a lot of flexibility in structural design.

Based on the clarification of the basic structure of the 2D-ES, we consider executing a periodic structural design for the empty space (ES) part as shown in Fig. 1, that is, assembling multilayer graphene spacers within a certain size of the ES part according to different numbers of periods. It should be noted that Fig. 1 is only used to demonstrate the structural features of a multilayer graphene with the periodic 2D-ES, which is not identical to the structure used for calculations, as will be explained in more detail in the subsequent section on calculation details. Insofar, we have completed our understanding of the core model in this study.

In this study, the assessment of the thermal transport capacity of the system, that is, the calculation of thermal conductivity, was mainly achieved by the homogeneous non-equilibrium molecular dynamics (HNEMD) method [28] based on the linear response theory, which is widely used in the study of thermal conductivity of nanomaterials [29–32]. This method realizes the calculation of thermal conductivity by simplifying the thermal transport process into a mechanical simulation combined with the Green–Kubo formula [33,34]:

$$\kappa_i(t) = \frac{\langle Q_i(t)\rangle_{ne}}{TVF_{ei}} = \frac{1}{t}\int_0^t \frac{\langle Q_i(\tau)\rangle_{ne}}{TVF_{ei}}d\tau \quad (i = x, y) \tag{1}$$

where T and V are the temperature and volume of the system, Q_i is the component of the heat flow vector $\vec{Q} = \sum_i \sum_{j\neq i} (\vec{r}_{ij} \otimes \frac{\partial U_j}{\partial \vec{r}_{ji}}) \cdot \vec{v}_i$ along the direction of i. F_{ei} is the scalar form of the driving force parameter used to generate the homogeneous heat flow along the i direction, and in this study the x and y directions correspond to the fast and slow axes, respectively. Further, by constructing the virial-velocity correlation function in a non-equilibrium steady state, the spectral decomposition value of thermal conductivity in the frequency domain can be obtained:

$$\kappa_i(\omega) = \frac{q_i(\omega)}{TVF_{ei}} = \frac{2\tilde{\vec{K}}_i(\omega)}{TVF_{ei}} \quad (i = x, y) \tag{2}$$

where $\tilde{\vec{K}}_i(\omega)$ is the result of the Fourier transform of the virial-velocity correlation function along the i direction. In addition, for the in-plane thermal conductivity, different sources of contribution can be obtained by distinguishing the in-plane and out-of-plane modes, which is important for the study of the phonon mechanism [35,36]. Specifically, the in-plane thermal conductivity can be divided into an in-plane portion dominated by transverse and longitudinal phonons, and an out-of-plane portion dominated by flexural phonons.

The large-scale MD simulations performed in this study were implemented based on the highly efficient Graphics Processing Unit Molecular Dynamics (GPUMD) package [36–39]. The interactions between the carbon atoms within the layer were described by the optimized Tersoff potential [40], and the vdW interaction between the layers was modeled uniformly by the following 12-6 Lennard-Jones (L-J) potential:

$$V(r_{ij}) = 4\chi\varepsilon\left[\left(\frac{\sigma}{r_{ij}}\right)^{12} - \left(\frac{\sigma}{r_{ij}}\right)^{6}\right] \tag{3}$$

where χ is the interface coupling strength, ϵ and σ are taken as 2.39 meV and 0.314 nm respectively [41]. A uniform time step of 1 fs was used, and the periodic and free boundary conditions were adopted in the in-plane and out-of-plane directions, respectively. After determining the above basic simulation conditions, the following adequate thermal equilibrium will be performed at the beginning of each set of MD simulations. Specifically, the system was firstly equilibrated for 1 ns (1 million time steps) at 10 K and zero pressure under the NPT system of the Berendsen thermostat. Then the system was heated to 300 K within the next 1 ns, and finally the NPT equilibration was continued at that temperature for 1 ns. Then, specific calculations and post-processing can be performed according to different MD methods to obtain the final results.

In the HNEMD method, the value of the driving force parameter F_e is crucial to determine whether the system can achieve a complete linear response with the desired signal-to-noise ratio. The nice thermal conductivity results are reflected in its good convergence over the simulation time, which is also the premise for ensuring the rationality of the assessment of the thermal transport properties under the HNEMD method. After the adequate tests in Figure S1.(a) (Supplementary materials), the parameter value of $F_e = 0.1\ \mu m^{-1}$ was determined in this study. From Figure S1.(b–c), it is also easy to see that only two to three independent sets of simulations were required to obtain the desired statistical accuracy by the HNEMD method with sufficient simulation time. Insofar, the basic scheme used for the thermal conductivity assessment is finalized, which is also the core calculation method throughout the next study.

Next, a series of size effect analysis was performed to save unnecessary computational expenses while ensuring the accuracy and precision of the calculation. In fact, it has been shown that a sufficiently large system size in the HNEMD method is fundamental to ensure good statistical precision of the thermal conductivity results [42]. In the multilayer graphene with periodic 2D-ES as shown in Fig. 1, the object of study regarding the size effect will be guaranteed to be a fixed length of 20.74 nm along the y direction due to the large space requirement of the structural design. On this basis, we constructed seven structures with uniformly spaced in-plane sizes along x axis from 5.99 nm to 23.94 nm with the total number of atoms ranging from

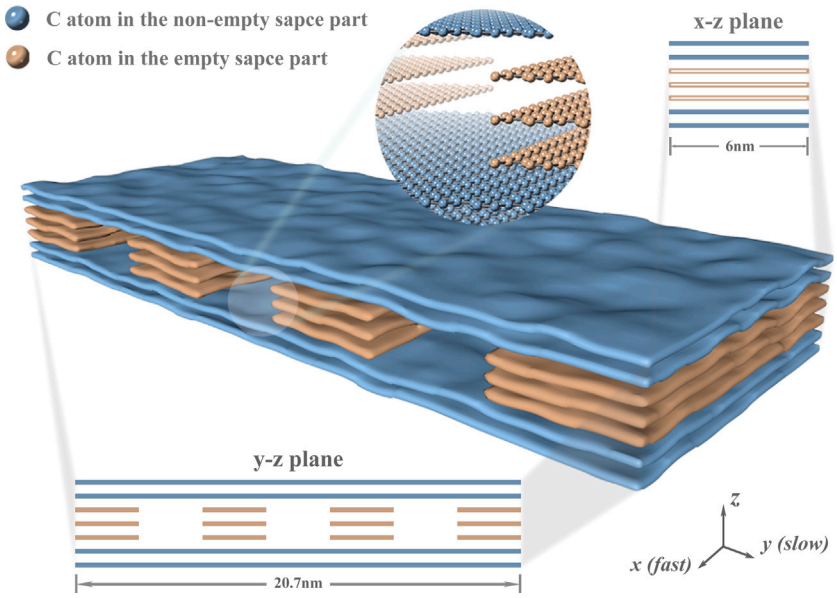

Fig. 1. Schematic diagram of a multilayer graphene structure with periodic 2D-ES, containing a perspective view of the structure as a whole, a zoomed-in view of the local atoms, and two side views that can show differences in the direction. Note that the hollow rectangle in the ES part on the side view of the xz plane is a visual representation of the structural discontinuity.

Table 1
Structural information for a seven-layer graphene model with a three-layer 2D-ES with different periodic natures.

	Number of periods	Period length (nm)	Interface density (nm^{-1})	Number of atoms
EG_1	12	1.725	1.159	25344
EG_2	8	2.588	0.773	25344
EG_3	6	3.450	0.580	25344
EG_4	3	6.900	0.290	25344
EG_5	2	10.350	0.193	25344
EG_6	1	20.700	0.097	25344

25,344 to as high as 10^5 order of magnitude. As shown in Figure S2, it is found that the thermal conductivity results remain stable with the change of sizes in the x-direction along both the fast and slow axes, which indicates that the in-plane size of 5.99 nm × 20.71 nm can meet the requirements of accuracy and precision of the thermal conductivity calculation results under the HNEMD method. Insofar, we have completed the entire discussion on the model and the method. The specific structural information of the model used for the next study of in-plane anisotropic thermal conductivity is shown in Table 1, and its specific structural schematic is shown in Figure S3.

3. Results and discussion

Herein, the anisotropic behavior of the in-plane thermal conductivity of multilayer graphene with periodic 2D-ES is investigated, where the independent variables are the number of layers in the ES part and the period length reflecting the nature of its specific periodic distribution. It should be noted that we further introduce the interface density, which corresponds one-to-one with the period length and characterizes the number of interfaces brought about by the 2D-ES within a certain length range. Fig. 2(a) plots the variation of the thermal conductivity of the structures with the period length (or interface density) in two different directions along the fast and slow axes for ES parts of 1, 3, and 5 layers, respectively. Firstly, along the slow axis, the thermal conductivity κ_s shows a clear overall decreasing trend over the whole range of period lengths, even though there are global anomalous maximum [27]. This is due to the fact that an increase in the period length of the 2D-ES implies a decrease in the interface density, which also means that the boundary phonon scattering from the interface perpendicular to the thermal transport direction is diminished. But more importantly, the low-frequency, long-wavelength phonons that dominate the thermal transport will cause a significant reduction in thermal conductivity due to the wider and more impenetrable cavity, which is the key to the overall decreasing trend in thermal conductivity along the slow axis in Fig. 2(a). Focusing next on the thermal conductivity κ_f along the fast axis, it shows an overall trend of increasing with period length along the opposite trend to κ_s. Structurally, the longitudinal graphene arrangement along the x direction in the ES part allows for good continuity of phonon transport without considering the transport across the 2D-ES. As a result, the thermal conductivity κ_f shows a relatively stable upward trend overall as the interface density decreases. And when the structure has more layers of 2D-ES, the more significant ES effect makes the above-mentioned change trend of thermal conductivity in both directions more stable.

Before considering the anisotropic thermal conductivity caused by the periodic 2D-ES, the effect of the difference in orientation of the multilayer graphene itself needs to be excluded. To this end, by calculating the thermal conductivity of the pristine seven-layer graphene along both x and y directions, it can be found that the effect of the orientation difference on the thermal conductivity is almost negligible, as shown in Figure S4. Further, from the lateral performance of the in-plane thermal conductivity anisotropy ratio γ in Fig. 2(b), it can be found that γ shows an almost stable increasing trend with increasing period length, which originates from the opposite trend of thermal conductivity along the fast and slow axis in Fig. 2(a). From a longitudinal point of view, it is clear that the coverage of γ is larger in structures with more layers of 2D-ES, which again strongly confirms the decisive role of periodic 2D-ES in this significant anisotropy. As shown in Fig. 2(c), compared to some typical 2D and quasi-2D structures, multilayer graphene with periodic 2D-ES can achieve a high in-plane thermal conductivity anisotropy ratio of $\gamma \approx 4.1$ while making γ relatively uniformly over a wide range of about $1.3 \sim 4.1$, which also possesses the basic conditions for an ideal tunable anisotropic thermal conductivity device conditions.

For the anisotropy of thermal conductivity of nonmetallic materials dominated by phonon contributions, the structural features describing their atomic distribution often give the intuitive qualitative explanation. As shown in Fig. 1, the 2D-ES setup is inherently directional,

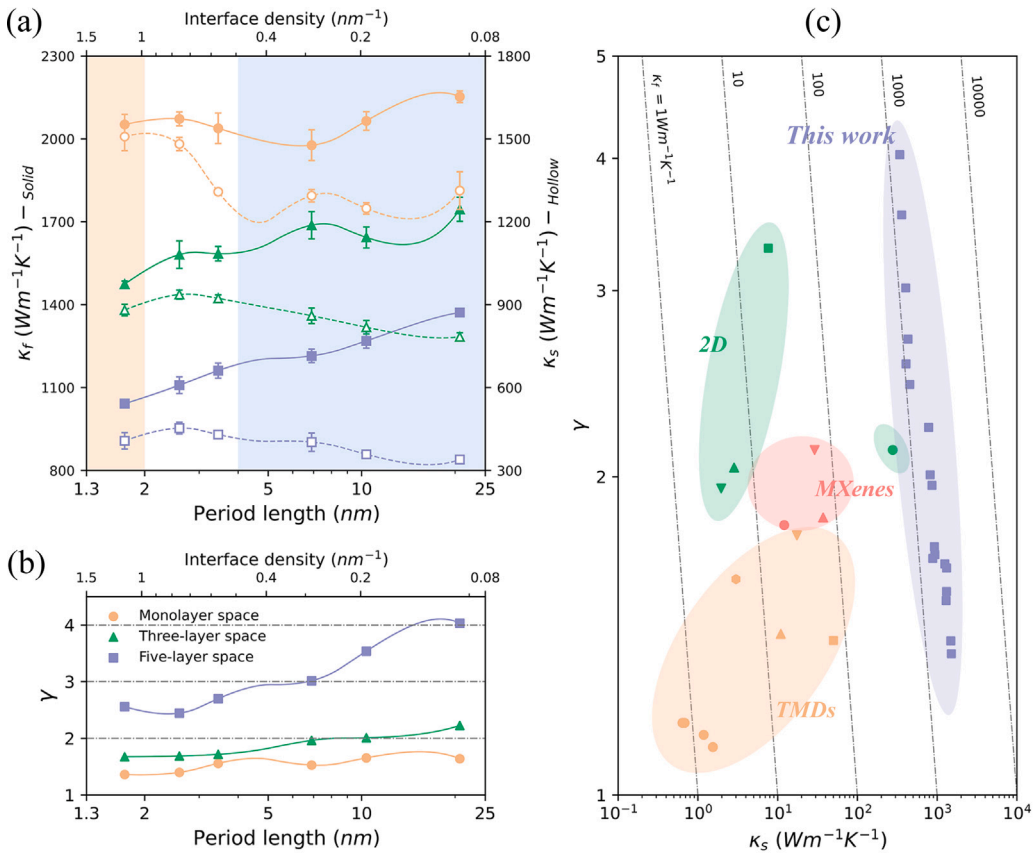

Fig. 2. Some results of in-plane anisotropic thermal transport in multilayer graphene with periodic 2D-ES. (a) Variation of in-plane thermal conductivity with period length (or interface density) at 300 K for seven layers of graphene with different layers of periodic 2D-ES along the fast (x-direction, solid markers) and slow (y-direction, hollow markers) axes, respectively. (b) Relationship between the in-plane thermal conductivity anisotropy ratio γ and the period length (or interface density) of seven-layer graphene with periodic 2D-ES of different number of layers. (c) Comparison between the in-plane thermal conductivity κ_f, κ_s, and γ of different quasi-2D materials, including typical 2D materials represented by black phosphorus [13–15], MXenes [21], and TMDs [16–20].

which is reflected by the difference in the distribution characteristics of graphene in the ES part along both x and y directions. Specifically in terms of the geometry of the interfaces, the former is longitudinally coherent, while the latter is blocked by several interfaces on the whole, which is the fundamental structural basis for the existence of significant anisotropy. In addition, the different periodicity exhibited by the 2D-ES distribution subtly provides opposite effects on the phonon transport of these two, which becomes the basis for the realization of a large-range anisotropy ratios in thermal conductivity.

Next, the thermal conductivity results of multilayer graphene with three-layer periodic 2D-ES are further analyzed from the perspectives of refinement to different frequency bands of phonon contributions and differentiation of in-plane and out-of-plane phonon contributions, as shown in Fig. 3(a–c). Also, the cumulative functions of thermal conductivity with respect to phonon frequencies are statistically and plotted in Fig. 3(d–f) based on the above results, which can effectively compensate for the lack of spectral thermal conductivity for the overall results analysis of the full frequency band. It should be noted here that the analysis in this part of the current study specific to different periodic structures is only focused on κ_f, while for κ_s only the overall comparison with κ_f is given, and a more detailed and interesting analysis of κ_s is given in our previous work [27]. Firstly, from the overall results, the differences in the periodic nature of the samples affect the thermal conductivity mainly through the effect on the characteristic peak value of the spectral thermal conductivity, and have little effect on the overall shape such as its location of the peak. Moreover, compared to the spectral thermal conductivity results along the slow axis indicated by the blue shaded area, the lower frequency phonons clearly have a higher percentage of the thermal conductivity contribution, which also implies that the effect of the difference in periodicity on κ_f is dominated by the low-frequency phonons. From the results of the total spectral thermal conductivity of the six structures with different periodic 2D-ES along the fast axis indicated by the different color curves in Fig. 3(a), the contribution of low-and-mid frequency phonons is absolutely dominant, which is highlighted by the two significant peaks appearing around 8 THz and 28 THz. Further, as shown in Fig. 3(b) and (e), the in-plane spectral thermal conductivities results of EG_1 to EG_6 are close to each other at lower overall values and do not show an effective gradient difference. However, the out-of-plane results in Fig. 3(c) and (f) are quite different, where the high similarity of the overall shape to the total spectral thermal conductivity and the apparently higher absolute peak together assert a dominant position in the thermal conductivity contribution. From EG_1 to EG_6, two characteristic peaks of the out-of-plane spectral thermal conductivity increase with the decrease of the interface density, which fully reflects the suppression effect of the interface scattering on the thermal transport.

The study of thermal conductivity anisotropy focuses on comparing the results of spectral thermal conductivity along two different directions in Fig. 3. From Fig. 3, it can be found that a very important difference between the two is whether the dominant term contributing to the thermal conductivity is the in-plane or out-of-plane component. Specifically, the in-plane component of the thermal conductivity along the fast axis is only about 20% higher than that along the slow axis, while the out-of-plane component is up to about 200% higher, which is also reflected in the severe weakening effect of the out-of-plane spectral thermal conductivity in the low-frequency band along the slow axis in Fig. 3(c). More intuitively, from the results of the absolute percentage of the in-plane and out-of-plane thermal conductivity components in

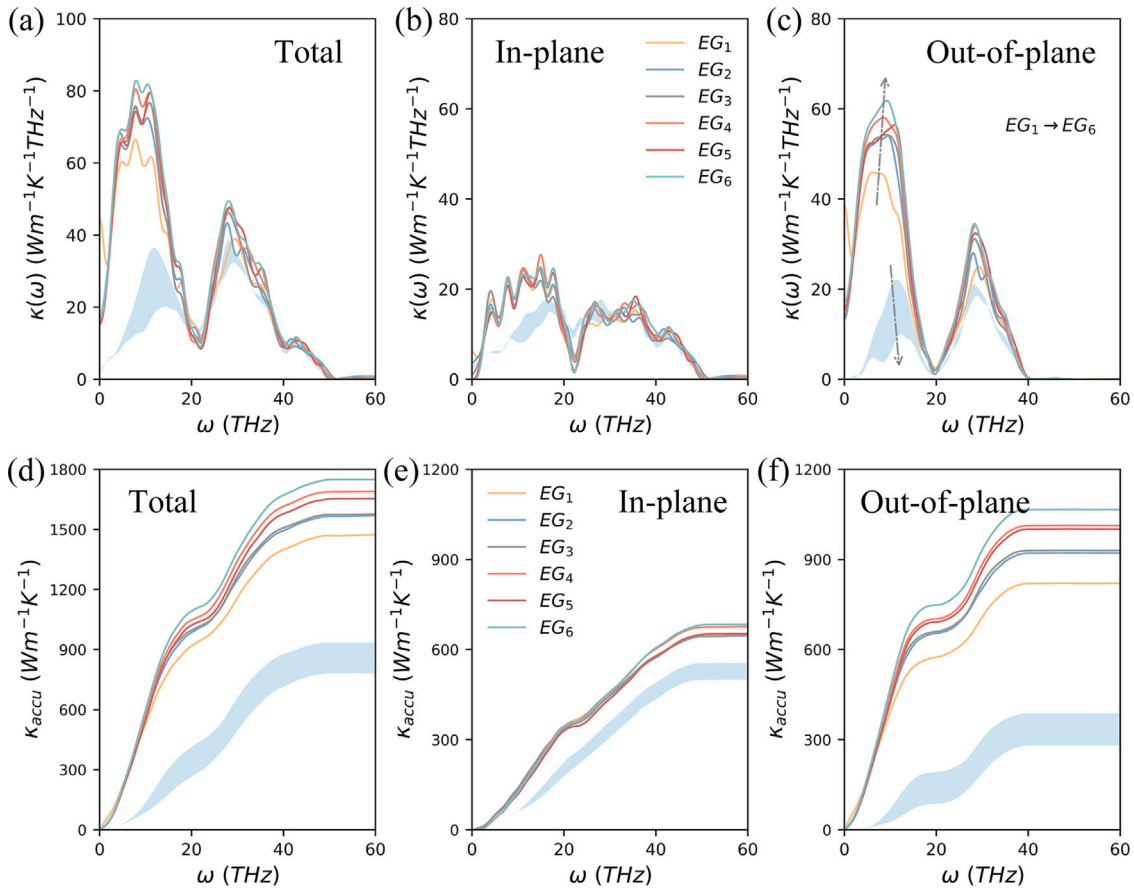

Fig. 3. The results of (a) spectral thermal conductivity and its (b) in-plane and (c) out-of-plane decomposition along the fast axis for EG_1 to EG_6 (structural information is shown in Table 1), and the corresponding (d–f) cumulative values of thermal conductivity versus the phonon frequency. Here, the blue shaded part in each subplot indicates the range of variation of the corresponding thermal conductivity along the slow axis. Note that the arrows in (c) are indications from EG_1 to EG_6. (For interpretation of the references to color in this figure legend, the reader is referred to the web version of this article.)

Figure S5, it can be observed that even though the out-of-plane stacking of multilayer graphene largely suppresses the contribution of out-of-plane phonons to thermal transport, it still does not change the dominance of out-of-plane phonons. This feature remains along the fast axis from EG_1 to EG_6, while the slow axis becomes an in-plane phonon dominated mode due to the influence of the 2D-ES across the thermal transport direction and the main frequency region corresponding to the peak position is more towards the higher frequency band. This explains the overall differential effect of the periodic 2D-ES on the thermal conductivity of multilayer graphene along two different directions above, which is the objective reason for the existence of anisotropic thermal conductivity.

Next, in order to give a clearer picture of the intuitive difference in spectral thermal conductivity in different directions for structures with different periodic properties and thus derive the essential source of anisotropy, the spectral thermal conductivity difference and its in-plane and out-plane decomposition results are plotted in Fig. 4, where the difference is defined as $\Delta\kappa = \kappa_f - \kappa_s$. Although there are negative values in the low-and-mid frequency around 20 THz, which means that the thermal conductivity along the fast axis is smaller than that along the slow axis, the spectral thermal conductivity of the fast axis is still absolutely superior to that of the slow axis, both in terms of the range of frequency bands covered and the magnitude of the difference in spectral thermal conductivity. And the decomposition results in Fig. 4(b–c) further illustrate that the thermal conductivity anisotropy is dominated by out-of-plane low-and-mid frequency phonons. Importantly, the dominant thermal conductivity anisotropy of 0 $\sim$ 20 THz with increasing period length (from EG_1 to EG_6) exhibits a clear trend of peak enhancement and significantly wider bandwidth, which determines the trend of monotonically increasing γ. The core reason for this result is that the effect of the periodic nature of the 2D-ES on the characteristic peaks in the low-and-mid frequency bands of the spectral thermal conductivity in different directions varies monotonically and with opposite trends, as shown in Fig. 3(c). Also, the slight rightward shift of the characteristic peak of $\kappa_s(\omega)$ contributes to some extent to the wider bandwidth of it. In fact, the key properties of phonon thermal transport in this band are macroscopically attributed to the following two aspects: (i) the relative relationship between the direction of thermal transport and the position of the 2D-ES, which is the premise of the study of thermal conductivity anisotropy, and (ii) the periodic nature that determines the way that 2D-ES arranged, that is, the period length or interface density, which is the core element that allows the modulation of phonon transport. This not only confirms the validity of the previous qualitative understanding of the results, but also shows that the study is essentially a successful case of achieving a wide range of anisotropic thermal conductivity through interface design for phonon transport modulation based on the directionality of the structure itself.

In order to further explore the underlying physical origin of the above-mentioned thermal conductivity anisotropy, the phonon level analysis is valid and cannot be neglected. In low-dimensional nanostructures containing interfaces introduced by such as the 2D-ES, frequent scattering of phonons during transport, including phonon-interface scattering and phonon–phonon scattering, tends to manifest itself in the form of phonon localization, which then severely affects the thermal conductivity of the system. The phonon participation rate (PPR) is an effective indicator of the phonon localization effect, which

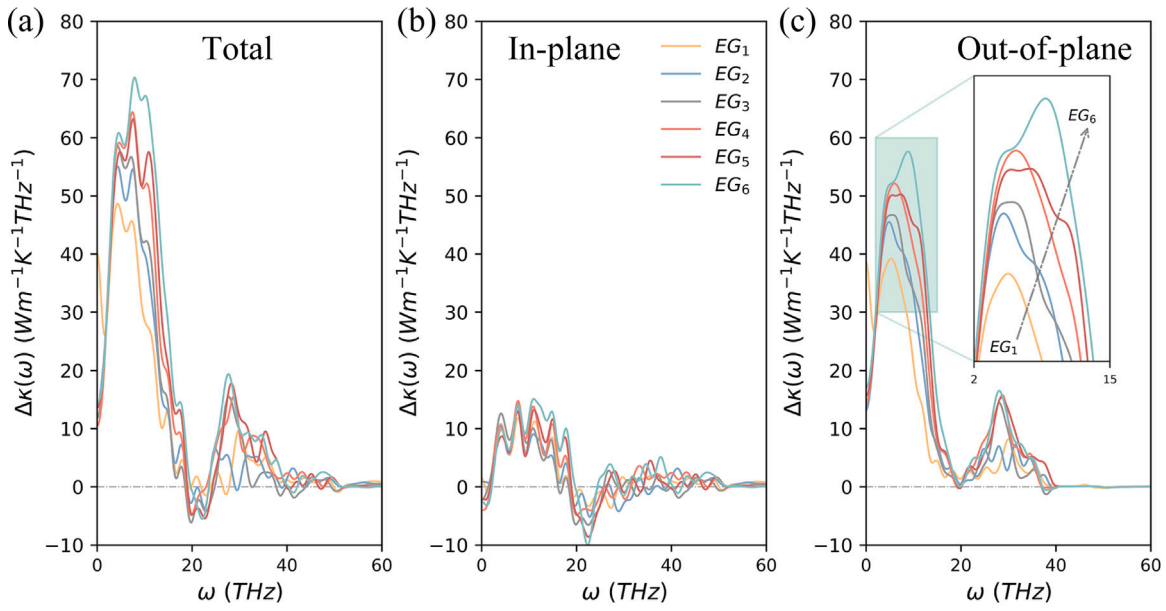

Fig. 4. The difference between the (a) total spectral thermal conductivity along the fast and slow axes, i.e., $\Delta\kappa = \kappa_f - \kappa_s$, and the phonon frequency for EG_1 to EG_6, and also gives the results of (b) in-plane and (c) out-of-plane decomposition results. The inset in (c) shows the amplification of the low-frequency band of 2 THz ~ 15 THz.

can be calculated by the MD method in the case of implicitly including non-harmonic scattering of all orders [43]:

$$PPR(\omega) = \frac{1}{N}\frac{\left(\sum_i PDOS_i^2(\omega)\right)^2}{\sum_i PDOS_i^4(\omega)} \tag{4}$$

where N is the number of atoms, and $PDOS_i(\omega)$ is the result of the phonon density of states (PDOS) of atom i calculated by:

$$PDOS_{i\alpha}(\omega) = \int_{-\infty}^{+\infty} \langle v_{i\alpha}(t)v_{i\alpha}(0)\rangle e^{-2\pi i\omega t}dt \quad (\alpha = x, y, z) \tag{5}$$

This is obtained based on the velocity auto-correlation function (VACF) $\langle v_{i\alpha}(t)v_{i\alpha}(0)\rangle$ of atoms in different directions, reflecting phonon activity in different modes.

According to the above method, the vibration spectra of the six structures from EG_1 to EG_6 at 300 K and their in-plane and out-plane decomposition results are calculated and plotted in Figure S6. From the PDOS results, it can be found that the activity of the low-frequency phonons that dominate the thermal conductivity anisotropy is mainly concentrated in the out-of-plane part, which is consistent with the previous results on the spectral thermal conductivity. A characteristic peak exists in the low frequency band of 8 THz ~ 15 THz of the out-of-plane PDOS, and its peak shows a gradual increase with the decrease of the interface density in the system. Further, in Fig. 5(b), four structures EG_1, EG_2, EG_4, and EG_6, which can fully characterize the trend of γ changes, are represented to show the calculated results of their PPR in the ES part. On the whole, although the atomic scale of the ES part is the same for the four representative structures, the differences in the periodic arrangement ways lead to quite different phonon activity.

For this purpose, the spectral thermal conductivity ranges of the six structures in both directions are plotted in Fig. 5(a), and the respective dominant frequency intervals are highlighted. In the dominant frequency band of κ_f from 4 THz to 12 THz, the phonon activity in the ES part generally maintains a high level of participation rate. Meanwhile, the PPR of ES parts from the EG_1 to EG_6 also shows a monotonically increasing trend, which is a direct manifestation of the effect of the interface density on the phonon scattering intensity and well explains the κ_f results under the influence of the periodic arrangement of the 2D-ES. Similarly, in the dominant frequency band of κ_s from 8 THz to 18 THz, the phonon activity in the ES part is severely limited and significant localization occurs between 12 THz and 18 THz. After entering the dominant frequency band of κ_s from around 10 THz, the original pattern of the PPR in ES parts with the change of the interface density starts to change. Typically, the PPR of EG_6 plummeted, which means that the increase in period length blocks the transport of some long-wave phonons and thus creates a significant localization effect. The above discussion adequately illustrates the intrinsic physical mechanism of the variation of thermal conductivity in both directions with the periodic nature of the 2D-ES in multilayer graphene from the perspective of phonon activity, which also explains the fundamental source of the promising thermal conductivity anisotropy.

In addition, for the key issue of phonon scattering at the ES interface mentioned in the above analysis, the evaluation of the phonon mean free path (MFP) will be of great significance as an intuitive assessment of the phonon thermal transport capacity. Next, the spectral heat current decomposition method (SHC) based on the combination of HNEMD and non-equilibrium molecular dynamics (NEMD) will be used to achieve a targeted analysis of the respective contributions of phonon MFP in the full frequency domain and in-and-out decomposition of the plane in the studied system. The key to this approach is that the phonon MFP (λ) in an infinite system can be defined by the ratio of diffusion thermal conductivity to ballistic thermal conductivity [30,44] for further generalization in the full frequency domain are:

$$\lambda = \frac{\kappa}{G} \quad , \quad \lambda(\omega) = \frac{\kappa(\omega)}{g(\omega)} \tag{6}$$

where κ and $\kappa(\omega)$ are the thermal conductivity of the system and its spectral decomposition results obtained by the HNEMD-SHC method, respectively, and G and $g(\omega)$ are the thermal conductivity and its spectral decomposition results obtained by the NEMD-SHC method. The details and results of the NEMD method are described in S7.

To this end, the phonon MFP and its in-plane and out-of-plane decomposition results along both the fast and slow axes for EG_1, EG_2, EG_4, and EG_6 are representative plotted in Fig. 6. The phonon MFP in both directions along the fast and slow axes show significant differences in the key frequency band dominating the thermal transport. Comparing the phonon MFP in different directions, the significantly larger value along the fast axis direction implies a stronger transport capacity of phonons, that is, a higher thermal conductivity. There is almost no difference between the in-plane components of the phonon MFP along the two different directions in the 4 THz ~ 15 THz dominant frequency band of thermal conductivity, however, there is a significant gap in

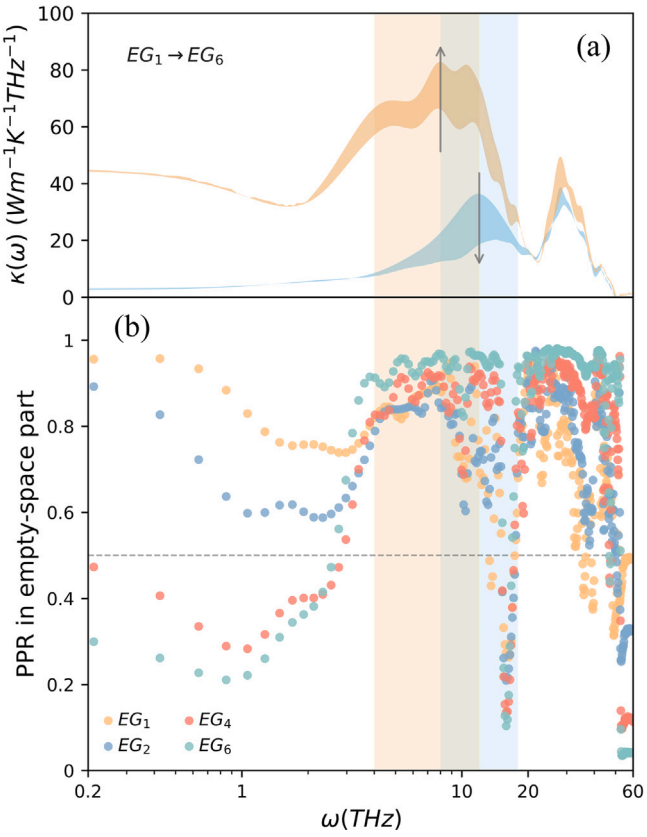

Fig. 5. (a) Spectral thermal conductivity versus phonon frequency for EG_1 to EG_6 along the fast axis (orange region) and slow axis (blue region), respectively, where the arrows are indicative of the transition from EG_1 to EG_6. (b) Phonon participation rate versus phonon frequency in the ES part in EG_1, EG_2, EG_4, and EG_6, where the representative structures are chosen so that the results can be presented more clearly. The dashed line is the horizontal reference line with $PPR = 0.5$ used to distinguish whether the phonons are localized or not. The longitudinal colored shaded regions indicate the frequency intervals of the dominant spectral thermal conductivity in each of the two directions. (For interpretation of the references to color in this figure legend, the reader is referred to the web version of this article.)

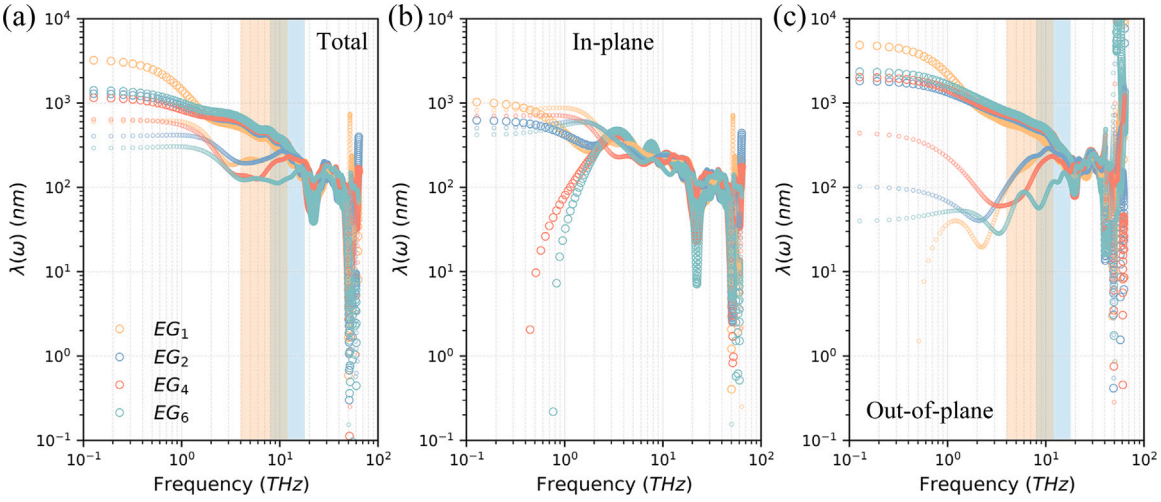

Fig. 6. The relationship between (a) the spectral phonon mean free path (MFP) $\lambda(\omega)$ and its (b) in-plane and (c) out-of-plane decomposition results with phonon frequency for four representative systems EG_1, EG_2, EG_4, and EG_6 along the fast (larger marker) and slow (smaller marker) axes, respectively. The dominant frequency intervals of κ_f and κ_s are marked with orange and blue shaded areas in both (a) and (c), respectively, to facilitate the targeted analysis of phonon MFP. (For interpretation of the references to color in this figure legend, the reader is referred to the web version of this article.)

the out-of-plane components in Fig. 6(c). When the interface brought by the 2D-ES is perpendicular to the thermal transport direction, the low-frequency out-of-plane phonons that have an effective dominant contribution to thermal conductivity are subjected to a stronger scattering effect, which is embodied in the phonon MFP that is about 5 times lower than the fast axis. While justifying the results in Fig. 3, this further reflects the underlying mechanism of the existence of thermal conductivity anisotropy. In addition, the variation of thermal conductivity along the fast axis due to the periodic nature can also be clearly and intuitively explained by the monotonic variation of the phonon MFP in the dominant frequency band. Moreover, it is clear from the analysis that the almost opposite trend of the thermal

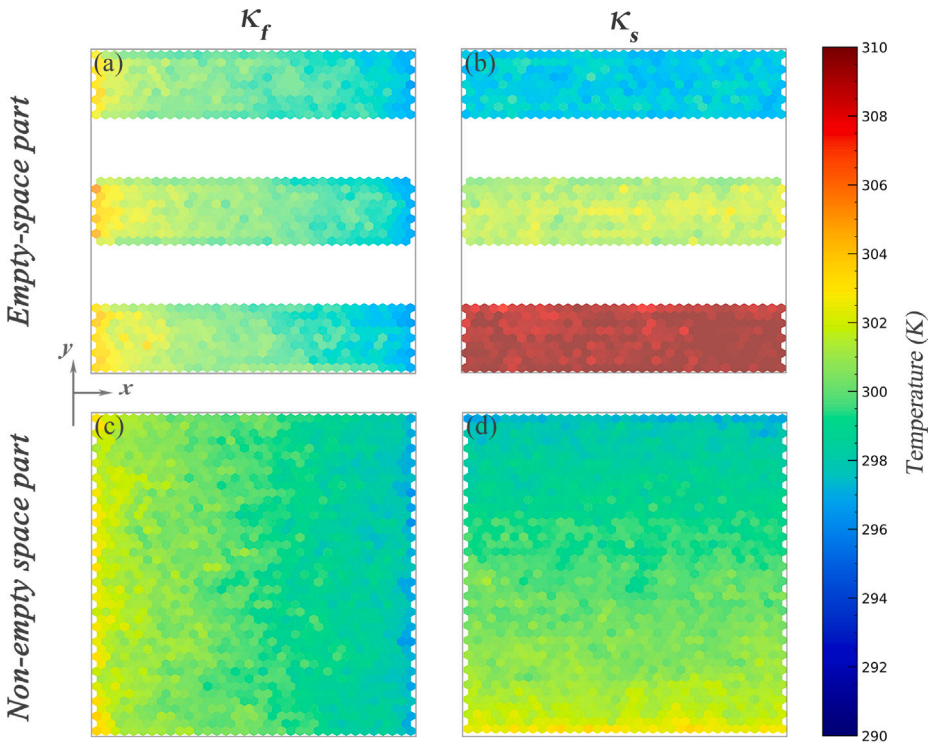

Fig. 7. Statistical results of the temperature spatial distribution of the ES part and the non-ES part in a square seven-layer graphene structure with three-layer periodic 2D-ES, which was obtained by the NEMD method of 310 K and 290 K for the heat source and the heat sink, respectively.

conductivity along the slow axis with respect to the periodic nature can be attributed to the reduction of the long-wavelength phonons involved in the transport due to the more impenetrable cavity brought about by the reduced interface density, which is the objective basis for the wide range of tunable thermal conductivity anisotropy. Finally, the length-dependent thermal conductivity results obtained by the SHC method are presented in S8, and they are in good agreement with the results based on the HNEMD method, which is another strong proof of the reliability of the results of this study.

In order to further verify the reliability of the previously obtained anisotropic thermal conductivity results and to obtain a clearer visualization of the anisotropic thermal transport, a square representative structure is selected and its spatial distribution of temperature during the thermal transport is shown in Fig. 7. Specifically, the results of the temperature spatial distribution during thermal transport along two different directions, fast axis (x) and slow axis (y), are calculated and counted separately under the same NEMD method configuration, including the ES part and non-ES part that are averaged separately in the out-of-plane direction. Firstly, an almost linear and uniform temperature distribution along the thermal transport direction can be observed in the non-ES part shown both in Fig. 7(c) and (d), which is a manifestation of the smoothness of the thermal transport process. However, the temperature distribution of the atoms in the ES part is quite different along the different thermal transport directions shown in Fig. 7(a–b). Along the fast axis, the ES part exhibits a smooth and unhindered temperature variation similar to that of the non-ES part. Along the slow axis, the broken distribution of temperature indicates that the presence of 2D-ES creates a significant hindering effect on thermal transport, due to the fact that 2D-ES perpendicular to the transport direction create energy barriers for phonons that are difficult to cross. The effect of the 2D-ES and its interface on the thermal transport along the fast axis seems to be limited only to the weakening of the amount of transfer medium, while that along the slow axis is fundamentally blocked, and this difference is also fundamental to the anisotropic thermal conductivity in present study.

4. Conclusion

In summary, the in-plane phonon thermal transport behavior in multilayer graphene with periodic 2D-ES was investigated by extensive large-scale MD simulations, and a large-range tunable anisotropic in-plane thermal conductivity with anisotropy ratios ranging from about 1.3 to 4.1 was found in it. The physical mechanisms involved are jointly explored through an analysis refined to the contribution of phonon frequencies and their in-plane and out-of-plane components to the thermal conductivity, combined with relevant discussions involving phonon localization effects, the phonon mean free path, and the spatial distribution of temperature. Firstly, the relative position between the thermal transport direction and the cavity is the fundamental premise for the existence of thermal conductivity anisotropy. Specifically, the blockage of thermal transport along the slow axis in the ES part is fatal and fundamental compared to the blocking effect on thermal transport along the fast axis. Then, the periodic nature that determines how the 2D-ES is arranged, that is, the period length or interface density, is the central element that allows for large-range modulation of the thermal conductivity anisotropy. Concretely, the different ways in which phonons cross the ES part make the monotonous change with the periodic arrangement of the 2D-ES show the opposite trend: as the period length increases (or the interface density decreases), (i) the weakening of phonon scattering at the interface directly leads to an overall upward trend in thermal conductivity along the fast axis; (b) the wider, more impenetrable 2D-ES prevents a portion of the long-wave phonons from continuing to perform effective transport and results in an overall reduction in thermal conductivity along the slow axis. The above opposite monotonic trend allows the thermal conductivity anisotropy ratio to cover a large range uniformly, which is a necessary condition for an ideal tunable anisotropic thermal conductor. This study comprehensively covers the key aspects from property exploration to mechanism analysis, providing new insights and inspiration for structural design-driven thermal property modulation of materials.

CRediT authorship contribution statement

Xin Wu: Conceptualization, Methodology, Software, Validation, Formal analysis, Investigation, Writing – original draft, Writing – review & editing, Visualization. **Qiang Han:** Resources, Supervision, Project administration, Funding acquisition.

Declaration of competing interest

The authors declare that they have no known competing financial interests or personal relationships that could have appeared to influence the work reported in this paper.

Data availability

Data will be made available on request.

Acknowledgments

The authors are grateful for support from the National Natural Science Foundation of China (11972160), Guangdong Basic and Applied Basic Research Foundation, China (2019A1515011900), Science and Technology Program of Guangzhou, China (202002030367).

Appendix A. Supplementary materials

Supplementary material related to this article can be found online at https://doi.org/10.1016/j.surfin.2022.102296.

References

[1] M.M. Waldrop, The chips are down for moore's law, Nature 530 (7589) (2016) 144–147.
[2] Y. Liu, Y. Huang, X. Duan, Van der waals integration before and beyond two-dimensional materials, Nature 567 (7748) (2019) 323–333.
[3] B. Jiang, S. Wang, J. Sun, Z. Liu, Controllable synthesis of wafer-scale graphene films: Challenges, status, and perspectives, Small 17 (37) (2021) e2008017.
[4] M.S. Alborzi, A. Rajabpour, A. Montazeri, Heat transport in 2d van der waals heterostructures: An analytical modeling approach, Int. J. Therm. Sci. 150 (2020) 106237.
[5] A. Rajabpour, Z. Fan, S.M. Vaez Allaei, Inter-layer and intra-layer heat transfer in bilayer/monolayer graphene van der waals heterostructure: Is there a kapitza resistance analogous? Appl. Phys. Lett. 112 (2018) 23.
[6] X.K. Chen, K.Q. Chen, Thermal transport of carbon nanomaterials, J. Phys.-Condes. Matter 32 (2020) 153002.
[7] K. Li, Y. Cheng, M. Dou, W. Zeng, S. Volz, S. Xiong, Tuning the anisotropic thermal transport in 110-silicon membranes with surface resonances, Nanomaterials 12 (2021) 1.
[8] B. Mortazavi, A. Lherbier, Z. Fan, A. Harju, T. Rabczuk, J.C. Charlier, Thermal and electronic transport characteristics of highly stretchable graphene kirigami, Nanoscale 9 (42) (2017) 16329–16341.
[9] S.E. Kim, F. Mujid, A. Rai, F. Eriksson, J. Suh, P. Poddar, A. Ray, C. Park, E. Fransson, Y. Zhong, D.A. Muller, P. Erhart, D.G. Cahill, J. Park, Extremely anisotropic van der waals thermal conductors, Nature 597 (7878) (2021) 660–665.
[10] W. Yu, X. Zhao, P. Jiang, C. Liu, R. Yang, Tunable anisotropic thermal transport in super-aligned carbon nanotube films, Mater. Today Phys. 20 (2021) 100447.
[11] X.K. Chen, X.Y. Hu, P. Jia, Z.X. Xie, J. Liu, Tunable anisotropic thermal transport in porous carbon foams: The role of phonon coupling, Int. J. Mech. Sci. 206 (2021) 106576.
[12] P. Jiang, X. Qian, X. Gu, R. Yang, Probing anisotropic thermal conductivity of transition metal dichalcogenides mx2 (m=mo, w and x=s, se) using time-domain thermoreflectance, Adv. Mater. 29 (2017) 36.
[13] Y. Zhao, G. Zhang, M.H. Nai, G. Ding, D. Li, Y. Liu, K. Hippalgaonkar, C.T. Lim, D. Chi, B. Li, J. Wu, J.T.L. Thong, Probing the physical origin of anisotropic thermal transport in black phosphorus nanoribbons, Adv. Mater. 30 (50) (2018) e1804928.
[14] A. Tabarraei, Thermal conductivity of monolayer hexagonal boron nitride nanoribbons, Comput. Mater. Sci. 108 (2015) 66–71.
[15] H. Liu, X. Yu, K. Wu, Y. Gao, S. Tongay, A. Javey, L. Chen, J. Hong, J. Wu, Extreme in-plane thermal conductivity anisotropy in titanium trisulfide caused by heat-carrying optical phonons, Nano Lett. 20 (7) (2020) 5221–5227.
[16] B. Wei, J. Liu, Q. Cai, A. Alatas, A.H. said, M. Hu, C. Li, J. Hong, Giant anisotropic in-plane thermal conduction induced by anomalous phonons in pentagonal pdse2, Mater. Today Phys. 22 (2022) 100599.
[17] L. Chen, W. Zhang, H. Zhang, J. Chen, C. Tan, S. Yin, G. Li, Y. Zhang, P. Gong, L. Li, In-plane anisotropic thermal conductivity of low-symmetry pdse2, Sustainability 13 (2021) 8.
[18] H. Jang, C.R. Ryder, J.D. Wood, M.C. Hersam, D.G. Cahill, 3D anisotropic thermal conductivity of exfoliated rhenium disulfide, Adv. Mater. 29 (2017) 35.
[19] Y. Chen, B. Peng, C. Cong, J. Shang, L. Wu, W. Yang, J. Zhou, P. Yu, H. Zhang, Y. Wang, C. Zou, J. Zhang, S. Liu, Q. Xiong, H. Shao, Z. Liu, H. Zhang, W. Huang, T. Yu, In-plane anisotropic thermal conductivity of few-layered transition metal dichalcogenide td-wte2, Adv. Mater. 31 (7) (2019) e1804979.
[20] Y. Wei, C. Deng, X. Zheng, Y. Chen, X. Zhang, W. Luo, Y. Zhang, G. Peng, J. Liu, H. Huang, W. Cai, Q. Ge, R. Zhang, X. Zhang, S. Qin, Anisotropic in-plane thermal conductivity for multi-layer wte2, Nano Res. 15 (1) (2022) 401–407.
[21] X.H. Zha, Q. Huang, J. He, H. He, J. Zhai, J.S. Francisco, S. Du, The thermal and electrical properties of the promising semiconductor mxene hf2co2, Sci. Rep. 6 (2016) 27971.
[22] A. Esfandiar, B. Radha, F.C. Wang, Q. Yang, S. Hu, S. Garaj, R.R. Nair, A.K. Geim, K. Gopinadhan, Size effect in ion transport through angstrom-scale slits, Science 358 (6362) (2017) 511–513.
[23] A. Keerthi, A.K. Geim, A. Janardanan, A.P. Rooney, A. Esfandiar, S. Hu, S.A. Dar, I.V. Grigorieva, S.J. Haigh, F.C. Wang, B. Radha, Ballistic molecular transport through two-dimensional channels, Nature 558 (7710) (2018) 420–424.
[24] A.K. Geim, Exploring two-dimensional empty space, Nano Lett. 21 (15) (2021) 6356–6358.
[25] Z. Zhang, Y. Guo, M. Bescond, J. Chen, M. Nomura, S. Volz, Coherent thermal transport in nano-phononic crystals: An overview, APL Mater. 9 (2021) 8.
[26] M. Nomura, R. Anufriev, Z.W. Zhang, J. Maire, Y.Y. Guo, R. Yanagisawa, S. Volz, Review of thermal transport in phononic crystals, Mater. Today Phys. 22 (2022) 100613.
[27] X. Wu, Q. Han, Maximum thermal conductivity of multilayer graphene with periodic two-dimensional empty space, Int. J. Heat Mass Transf. 191 (2022) 122829.
[28] D.J. EVANS, Homogeneous nemd algorithm for thermal conductivity appliccation of non-canonical linear response theory, Phys. Lett. 91 (9) (1982) 457–460.
[29] A.J. Gabourie, Ç. Köroğlu, E. Pop, Substrate-dependence of monolayer mos2 thermal conductivity and thermal boundary conductance, J. Appl. Phys. 131 (2022) 19.
[30] Z. Fan, H. Dong, A. Harju, T. Ala-Nissila, Homogeneous nonequilibrium molecular dynamics method for heat transport and spectral decomposition with many-body potentials, Phys. Rev. B 99 (2019) 6.
[31] P. Ying, T. Liang, Y. Du, J. Zhang, X. Zeng, Z. Zhong, Thermal transport in planar sp2-hybridized carbon allotropes: A comparative study of biphenylene network, pentaheptite and graphene, Int. J. Heat Mass Transf. 183 (2022) 122060.
[32] H. Dong, Z. Fan, P. Qian, T. Ala-Nissila, Y. Su, Thermal conductivity reduction in carbon nanotube by fullerene encapsulation: A molecular dynamics study, Carbon 161 (2020) 800–808.
[33] M.S. Green, Markoff random processes and the statistical mechanics of time-dependent phenomena. ii. irreversible processes in fluids, J. Chem. Phys. 22 (3) (1954) 398–413.
[34] R. Kubo, Statistical–mechanical theory of irreversible processes. i. general theory and simple applications to magnetic and conduction problems, J. Phys. Soc. Jpn. 12 (6) (1957) 570–586.
[35] X. Zhang, M. Hu, D. Tang, Thermal rectification at silicon/horizontally aligned carbon nanotube interfaces, J. Appl. Phys. 113 (19).
[36] Z. Fan, L.F.C. Pereira, P. Hirvonen, M.M. Ervasti, K.R. Elder, D. Donadio, T. Ala-Nissila, A. Harju, Thermal conductivity decomposition in two-dimensional materials: Application to graphene, Phys. Rev. B 95 (2017) 14.
[37] Z. Fan, Y. Wang, P. Ying, K. Song, J. Wang, Y. Wang, Z. Zeng, K. Xu, E. Lindgren, J.M. Rahm, A.J. Gabourie, J. Liu, H. Dong, J. Wu, Y. Chen, Z. Zhong, J. Sun, P. Erhart, Y. Su, T. Ala-Nissila, Gpumd: A package for constructing accurate machine-learned potentials and performing highly efficient atomistic simulations, 2020, arXiv:arXiv:2205.10046.
[38] Z. Fan, L.F.C. Pereira, H.-Q. Wang, J.-C. Zheng, D. Donadio, A. Harju, Force and heat current formulas for many-body potentials in molecular dynamics simulations with applications to thermal conductivity calculations, Phys. Rev. B 92 (9) (2015) 094301.
[39] Z.Y. Fan, W. Chen, V. Vierimaa, A. Harju, Efficient molecular dynamics simulations with many-body potentials on graphics processing units, Comput. Phys. Commun. 218 (2017) 10–16.

[40] L. Lindsay, D.A. Broido, Optimized tersoff and brenner empirical potential parameters for lattice dynamics and phonon thermal transport in carbon nanotubes and graphene, Phys. Rev. B 81 (2010) 20.
[41] A.K. Rappe, C.J. Casewit, K.S. Colwell, W.A. Goddard, W.M. Skiff, Uff, a full periodic table force field for molecular mechanics and molecular dynamics simulations, J. Am. Chem. Soc. 114 (25) (1992) 10024–10035.
[42] X. Gu, Z. Fan, H. Bao, C.Y. Zhao, Revisiting phonon-phonon scattering in single-layer graphene, Phys. Rev. B 100 (2019) 6.
[43] G.C. Loh, E.H.T. Teo, B.K. Tay, Phonon localization around vacancies in graphene nanoribbons, Diam. Relat. Mat. 23 (2012) 88–92.
[44] K. Sääskilahti, J. Oksanen, S. Volz, J. Tulkki, Frequency-dependent phonon mean free path in carbon nanotubes from nonequilibrium molecular dynamics, Phys. Rev. B 91 (2015) 11.